Research Square

Preprints are preliminary reports that have not undergone peer review.
They should not be considered conclusive, used to inform clinical practice,
or referenced by the media as validated information.

High-value reuse of coal gangue through fiber-reinforced pavement-base composites: Mechanical performance and model-based feasibility

Peng Huang
China University of Mining and Technology
Qihe Lan
ts24020138p31@cumt.edu.cn

China University of Mining and Technology
Erkan Topal
Curtin University
Hu Shao
China University of Mining and Technology
Zhenjiang You
China University of Petroleum, Beijing
Chengyi Zhao
Yunnan Phosphating Group Co., Ltd, Kunyang Phosphate Mine
Shuxuan Ma
China University of Mining and Technology

Article

Keywords: coal gangue, Solid waste reutilization, Fiber-reinforced composites, numerical simulation, sustainable systems

Posted Date: August 27th, 2026

DOI: https://doi.org/10.21203/rs.3.rs-10609299/v1

License: This work is licensed under a Creative Commons Attribution 4.0 International License.
Read Full License

Additional Declarations: No competing interests reported.

Version of Record: A version of this preprint was published at Scientific Reports on November 7th, 2026. See the published version at https://doi.org/10.1038/s41598-026-79281-9.

High-value reuse of coal gangue through fiber-reinforced pavement-base composites: Mechanical performance and model-based feasibility

Peng Huang[1], Qihe Lan*[1], Erkan Topal [6], Hu Shao[2], Zhenjiang You [4,5] ,Chengyi Zhao [3], Shuxuan Ma[1]

（1. Ministry of Education Key Laboratory of Deep Mining, School of Mining Engineering, China University of Mining and Technology, Xuzhou, Jiangsu 221116; 2.School of Mathematics, Jiangsu Center for Applied Mathematics (CUMT), China University of Mining and Technology, Xuzhou， 221116;3. Yunnan Phosphating Group Co., Ltd., Kunyang Phosphate Mine, Kunming, Yunnan, 650000; 4. School of Petroleum, China University of Petroleum-Beijing at Karamay, Karamay 834000, China;5.Gas and Energy Transition Research Centre, The University of Queensland, Brisbane, QLD 4072, Australia;6. WA School of Mines: Minerals, Energy and Chemical Engineering, Curtin University, Perth, WA 6102, Australia)

Corresponding author*: Qihe Lan; Email: ts24020138p31@cumt.edu.cn

Abstract: Coal-gangue-based pavement-base materials offer a promising route for large-scale solid-waste utilization. This study evaluated gangue–fly ash–cement–fiber mixtures containing 0.2–0.8% basalt fiber through mechanical testing, X-ray diffraction, scanning electron microscopy, and three-dimensional numerical simulation. Unconfined compressive and splitting tensile strengths increased as the fiber content increased from 0.2% to 0.6% and then decreased at 0.8%. The 0.6% mixture achieved the highest 28 d unconfined compressive and splitting tensile strengths of 14.47 and 1.51 MPa, respectively. In contrast, compressive resilient modulus decreased with increasing fiber content, indicating a strength–stiffness trade-off. The modeled settlement varied only slightly among the fiber-dependent parameter sets but was more sensitive to vehicle speed and traffic-load magnitude. XRD and SEM observations were consistent with continued reaction-product development, matrix densification, fiber–matrix contact, and possible crack bridging. Overall, 0.6% fiber provided the best strength performance within the tested range, while the numerical results provide comparative evidence for evaluating the pavement-scale response of the GFCF base layer and support the high-value utilization of coal gangue in pavement engineering.

Keywords: coal gangue; Solid waste reutilization; Fiber-reinforced composites; numerical simulation; sustainable systems

1 Introduction

As a byproduct of coal extraction and processing, coal gangue constitutes some 10–25% of raw coal production by mass and consists mainly of carbonaceous shale, mudstone, and a small proportion of coal[1–3]. The large-scale storage of coal gangue not only occupies land, destroys soil and pollutes the surrounding environment, but also has potential safety hazards such as spontaneous combustion. Therefore, improving the high-value utilization of coal gangue is essential for alleviating environmental pressure and promoting sustainable waste management systems.[4–7]. With the development of comprehensive utilization technology of resources, coal gangue is gradually regarded as a secondary resource and applied in the fields of power generation and brick making. However, most existing studies focus on material-level performance, while the system-level feasibility and deformation behavior under realistic service conditions remain insufficiently investigated.[8]. In a variety of utilization ways, coal gangue has been widely considered as a pavement base material because it can replace natural aggregate, and has gradually expanded from the early use of surface subsidence backfilling and land reclamation to chemical materials, road filling, and building materials[9,10]. Numerous experts and scholars have conducted extensive experimental investigations such as evaluating the mechanical properties of cement mortar incorporating calcined coal gangue as a cement substitute from both microscopic and macroscopic perspectives, while also identifying key factors influencing its performance[11–13]. Coal gangue has been widely used in the field of civil engineering, especially in the construction of highway subgrade and foundation cushion, and has been successfully applied in road and railway engineering in northern France, the Ruhr district of Germany, and Gloucester and Croydon of Britain[14]. With the continuous development of China's transportation infrastructure, coal gangue is increasingly used as roadbed filler and cushion material in highway engineering, and its mechanical properties can meet the design requirements of highway roadbed[15].

Coal gangue has better characteristics than some soft soils, such as ultimate bearing capacity, water permeability, and strength characteristics, and has achieved certain results as a building foundation material in land reclamation of mining areas [16–18]. The accumulation of coal gangue as mining waste in the mining area will cause serious environmental pollution. The use of coal gangue as roadbed filling has the advantages of convenient materials and large consumption, which can effectively alleviate the social and environmental problems caused by the storage of coal gangue in the mining area[19–21]. Cement concrete pavement is widely used in highways and urban roads, but it has defects such as brittleness and easy cracking. The incorporation of fiber can effectively improve its crack resistance, strength, and toughness[22]. The properties of coal gangue concrete mixed with different types of steel fibers were studied by experiments. The results show that the addition of steel fibers can effectively alleviate the brittleness and crack sensitivity of materials, and significantly improve their mechanical properties and frost resistance[23–25]. Development of C40 Ordinary Concrete Using Coal Gangue as a Complete Substitute for Natural Crushed Stone: mixed with coal gangue concrete, added fiber and mixing ratio, and then modified coal gangue concrete with single fly ash and mixed fly ash and mineral powder with different cement replacement rates. The coal gangue concrete obtained has high mechanical properties after modification[26]. Single coal gangue material has defects such as poor water stability and large strength fluctuation, and it needs to be modified by inorganic binder to improve its performance[27–29].

In this study, a gangue–fly ash–cement–fiber (GFCF) composite was developed as a high-value utilization pathway for coal gangue. Laboratory tests were conducted to evaluate the mechanical and deformation performance of GFCF mixtures with different fiber contents, and scanning electron microscopy was used to elucidate the reinforcement mechanisms. Furthermore, a three-dimensional numerical model was established to assess the deformation behavior of GFCF pavement base layers under traffic loading. This study aims to provide both material-level and system-level evidence for the feasibility of coal gangue reutilization in sustainable road infrastructure.

2 Basic Mechanical Properties of GFCF Pavement Base Material

2.1 Cement, fly ash, and basalt fiber

Coal gangue and fly ash were obtained from Yangcheng Coal Mine in Jining, Shandong Province, China. P.O. 42.5 ordinary Portland cement was used as the binder. Chopped basalt fiber with a nominal length of 12 mm was added externally. The archived batch properties of these materials are summarized in Table 1.

Table 1. Archived properties of cement, fly ash, and basalt fiber.

Material	Archived property	Value
Cement	Initial/final setting time	330/442 min
	Flexural strength, 3/28 d	4.3/7.4 MPa
	Compressive strength, 3/28 d	29.6/46.8 MPa
Fly ash	SiO2/Al2O3/Fe2O3	53.24/32.01/3.69%
	Density; loss on ignition	2.01 g cm^{-3}; 5.2%
Basalt fiber	Form and nominal length	Bundled monofilament; 12 mm
	Density; tensile strength	3.04 g cm^{-3}; 1265 MPa
	Water absorption; elongation	<0.1%; 3.01%

The GFCF mixture comprised ordinary Portland cement, fly ash, and chopped basalt fiber. Cement provided the primary hydraulic binding phase, whereas fly ash acted as a fine mineral component with particle-filling capacity and potential later-age pozzolanic reactivity. Basalt fiber was introduced as a discrete, non-corrosive reinforcement phase to bridge incipient cracks and redistribute tensile stress. A nominal fiber length of 12 mm was adopted to balance mechanical anchorage with dispersion during mixing. This subsection describes the constituent materials only. Published studies similarly indicate that fiber type and geometry must be selected for the specific stabilized matrix [30–32].

2.2 Basic physical properties of coal gangue

Following the test methods specified in the Specifications for Aggregate Test of Highway Engineering (JTGE42-2005) and Specifications for Geotechnical Test of Highway Engineering (JTG3430-2020), the key physical properties of the coal gangue were evaluated and are presented in Table 2.

Table 2 Basic physical properties of coal gangue

C_u	C_c	ω（%）	δ_{ef}（%）	$Q_a^{'}$	ρ_d（g / cm^3）	ω_b（%）	UCS^7（MPa）	UCS^{28}（MPa）
20.45	1.94	4.49	22.25	18.18	2.23	5.76	0.49	0.52

Where, Uniformity coefficient，C_u；curvature coefficient，C_c；water absorption，ω；free swelling ratio，δ_{ef}；crushing value，Q`a；maximum dry density，ρ_d；optimum moisture content，ω_b； 7d unconfined compressive

strength，UCS_7； 28d unconfined compressive strength，UCS_{28}

2.3 Basic chemical composition of coal gangue

The chemical composition of the coal-gangue sample was determined by X-ray fluorescence (XRF). Representative particles were crushed, dried at 60 °C for 24 h, ground, and sieved to <75 μm before tablet preparation and analysis. The results are summarized in Table 3. The relatively high combined SiO_2 and Al_2O_3 content indicates an aluminosilicate-rich material; however, chemical composition alone does not establish pozzolanic reactivity, which also depends on mineralogy, amorphous content, fineness, and activation conditions.

Table 3 Chemical element composition of coal gangue

ingredient	SiO_2 (%)	Al_2O_3 (%)	Fe_2O_3 (%)	CaO (%)	MgO (%)	K_2O (%)	Na_2O (%)	TiO_2 (%)	MnO_2 (%)	P_2O_5 (%)
content	63.60	20.71	6.46	0.70	1.86	2.61	0.55	1.03	0.05	0.17

As presented in Table 3, the coal gangue is dominated by $SiO_2$and Al_2O_3, which together account for more than 80% of the measured oxide composition. Other identified oxides include Fe_2O_3, K_2O, MgO, TiO_2, CaO, Na_2O, MnO_2, and P_2O_5.

2.4 Basic Mechanical Properties of GFCF Pavement Base Material

2.4.1 Experimental scheme design

The baseline formulation was selected from previous studies on inorganic-binder-stabilized coal-gangue and fiber-reinforced pavement materials [33–35]. Those studies informed the choice of aggregate gradation and binder proportions; the present work uses the selected formulation as a fixed reference matrix for evaluating basalt-fiber dosage.

The Talbot gradation exponent was fixed at n = 0.4, and the dry-mass ratio of coal gangue: fly ash: cement was 82:12:6. Basalt fiber was added at 0.2%, 0.4%, 0.6%, and 0.8% of the dry mixture mass. Specimens were tested after 7 and 28 d of curing. No 0% fiber control is presented in Figures 1- 3; therefore, all comparisons in this paper are restricted to the four tested fiber dosages.

2.4.2 GFCF Pavement Base Material Unconfined Compressive Strength

Cylindrical specimens (φ150 mm × 150 mm) were prepared in compliance with JTG E51-2009. The coal gangue was adjusted to its optimum moisture content of 5.76% and equilibrated for 4–6 h prior to static compaction at 1 mm/min, with pressure maintained for 40 minutes. After demoulding, the specimens were sealed and cured at 20 ± 2 °C. Unconfined compressive strength was measured after 7 and 28 days (Figure 1), calculated using the following equation:

$$A = \frac{\pi D^2}{4} \quad (1)$$

$$R_c = \frac{P}{A} \quad (2)$$

where R_c is unconfined compressive strength, MPa; P is peak failure load, N; A is cross-sectional area, mm²; calculated from diameter D, mm.

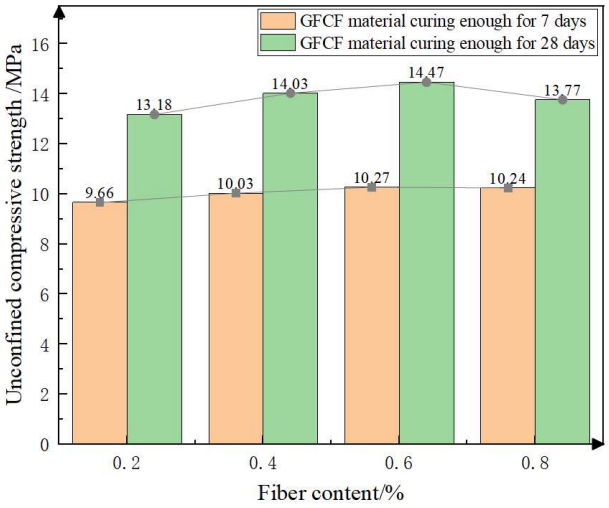


Figure 1 Unconfined compressive strength of GFCF pavement base material

As illustrated in Figure 1, the Unconfined compressive strength of the GFCF base material initially increases before decreasing with rising fiber content, a trend consistent at both 7- and 28-day curing ages. The maximum strengths, recorded at 0.6% fiber content for 7 days and 28 days curing periods, reached 10.27 MPa and 14.47 MPa, respectively. When the content of is 0.6 %, the increase rate is the fastest, and the compressive strength from 7d age to 28d age increases by 40.90 %. When the fiber content is 0.8 %, the increase rate is the slowest, and the compressive strength from 7d age to 28d age increases by 34.47 %.

2.4.3 Splitting Strength of GFCF Pavement Base Material

Splitting tensile strength was measured for the fiber-reinforced GFCF base material after 7 and 28 days of curing, in compliance with JTG E51-2009. The results, calculated via Equation (3), are presented in Figure 2.

$$R_i = \frac{2P}{\pi D h_3}\left(\sin 2\beta - \frac{f}{D}\right) \quad (3)$$

Where, R_i is the splitting strength, MPa; P is the peak pressure when the specimen fails, N; D is the specimen diameter, mm; f is the strip width, mm; h_3 is the height of the specimen after immersion, mm; β is the central angle corresponding to the strip width, °;

Because the test specimen is a cylinder specimen of 150mm×150mm, which belongs to a large specimen, the calculation formula can be simplified as follows:

$$R_i = 0.004178\frac{P}{h_3} \quad (4)$$

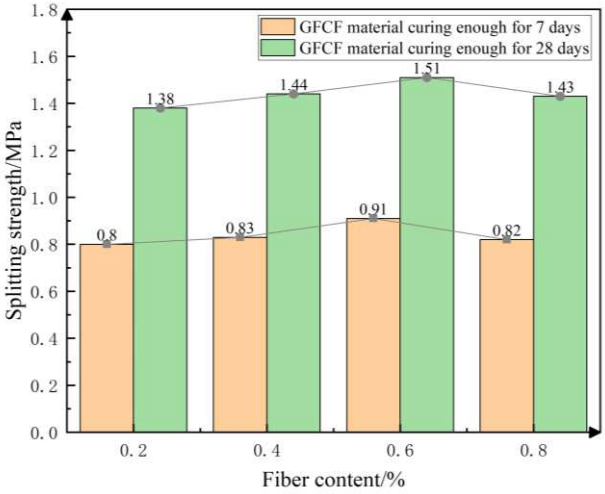


Figure 2 Splitting tensile strength of GFCF pavement base material

Figure 2 shows a nonlinear effect of fiber content on splitting tensile strength, with strength increasing up to 0.6% fiber and then declining at 0.8%. The 0.6% mixture achieved the highest values of 0.91 MPa at 7 d and 1.51 MPa at 28 d. The improvement at moderate dosage is consistent with fiber bridging and crack-arrest effects, whereas excessive fiber may cause agglomeration and structural heterogeneity. The higher 28 d strengths are mainly associated with continued hydration and matrix densification.

2.4.4 Compression modulus of GFCF pavement base material

Cylindrical specimens (ϕ 150 mm × 150 mm) of the GFCF base material were fabricated and moist-cured at constant temperature for 7 and 28 days in accordance with JTG E51-2009. Prior to testing, both end faces of the specimens were polished and leveled using an abrasive wheel, followed by the application of a fine layer of sand (0.25–0.5 mm) to ensure full contact during loading. The compressive modulus test of the GFCF mixture shall be carried out. The cyclic loading procedure was applied at a maximum load corresponding to 50%–60% of the mixture's unconfined compressive strength. A total of five loading-unloading cycles were conducted uniformly, and the readings of each loading and unloading shall be recorded. Resilient deformation l = reading under loading-reading under unloading. The resilient modulus (E_c) was calculated using Equation (5), with results shown in Figure 3.

$$E_c = \frac{ph}{l} \quad (5)$$

E_c——modulus of resilience in compression，MPa

p——specific pressure，MPa

h——specimen height，mm

l——specimen springback deformation，mm

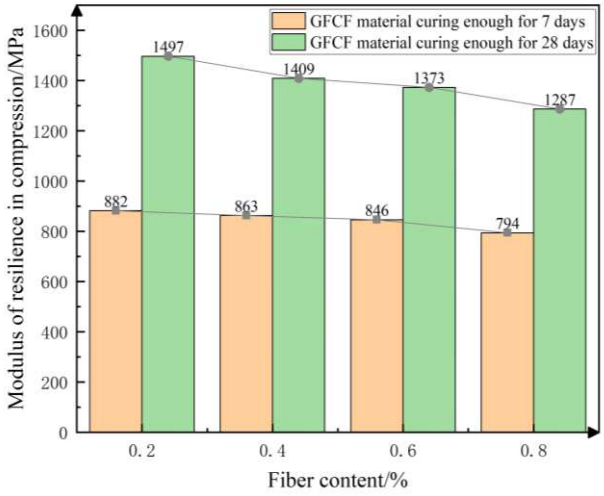


Figure 3 compressive resilient modulus of GFCF pavement base material

Figure 3 shows that the compressive resilient modulus decreased consistently as fiber content increased. From 0.2% to 0.8% fiber, the modulus decreased from 882 to 794 MPa at 7 d and from 1497 to 1287 MPa at 28 d. The results therefore indicate a reduction in resilient stiffness with increasing fiber dosage. The larger difference at 28 d may be associated with continued matrix development and stronger fiber-matrix interaction, which made the stiffness response to fiber dosage more distinct.

Considering the strength and resilient modulus results together, the 0.6% mixture provided the highest measured compressive and splitting tensile strengths, whereas increasing fiber content reduced resilient stiffness. Basalt-fiber addition therefore produced a strength-stiffness trade-off rather than a uniform improvement in all mechanical properties. Crack resistance was not measured directly in this study.

3 Simulation of road settlement law of GFCF-filled subgrade

3.1 Model establishment and basic parameters

The modeled road section comprised the pavement structure and the underlying subgrade, as illustrated in Figure 4. Across the section, the road width included traffic lanes, a median, hard shoulders, and soil shoulders. The fill subgrade was divided vertically into the upper roadbed, lower roadbed, upper embankment, and lower embankment. For light, medium, and heavy traffic, the upper roadbed occupied the upper 0–30 cm, the lower roadbed 30–80 cm, the upper embankment 80–150 cm, and the lower embankment the zone below 150 cm. For heavy or extremely heavy traffic, the corresponding lower-roadbed and upper-embankment ranges were 30–120 cm and 120–190 cm, respectively, with the lower embankment below 190 cm.

For a first-class highway, each traffic lane was taken as 3.75 m wide. A two-way, four-lane cross-section with a total pavement width of 24 m was adopted, exceeding the stated minimum width of 23.5 m. The pavement system was simplified into a surface layer, a GFCF base layer, and a subgrade-soil layer (Figure 4). The side-slope ratio was expressed as the ratio of slope height to horizontal width, as illustrated in Figure 5.

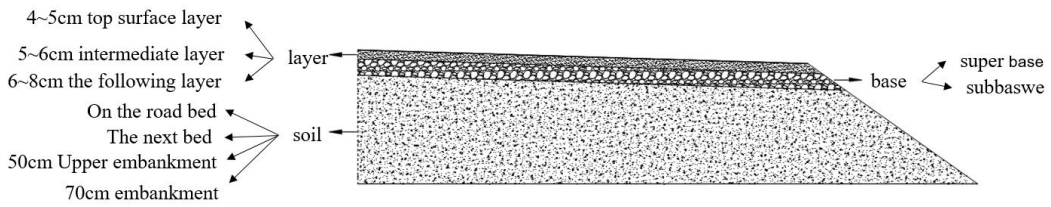


Figure 4 Schematic diagram of roadbed section structure

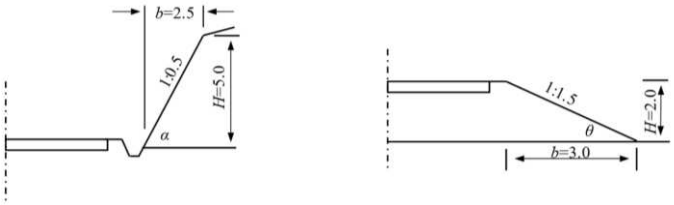


Figure 5 Schematic diagram of roadbed slope ratio (dimensions in meters)

The roadbed slope ratio depends on soil type, slope height, geological structure, and hydrogeological conditions, and it affects stability, earthwork volume, and construction difficulty. Following the Highway Subgrade Design Specification (JTG D30-2015), a slope ratio of 1:1.5 was adopted for the fine-grained-soil subgrade.

Based on the experimental results and the adopted highway geometry, the numerical model used a pavement width of 24 m, four traffic lanes of 3.75 m each, a side-slope ratio of 1:1.5, a 0.15 m surface layer, a 0.30 m GFCF base layer, and a 2.80 m subgrade-soil layer. The model geometry is shown in Figure 6.

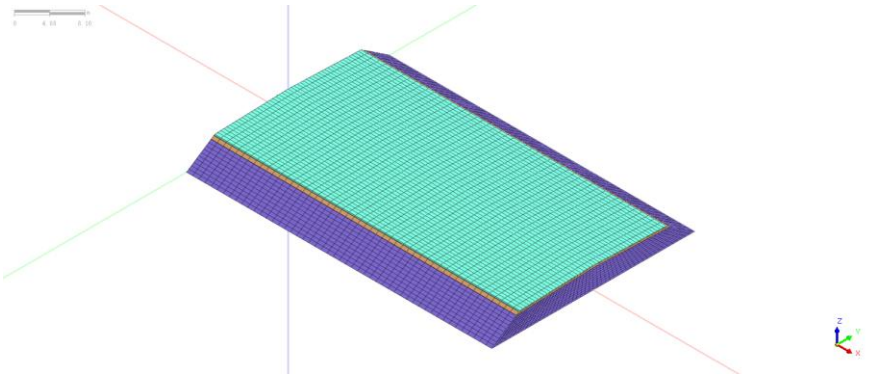


Figure 6 Numerical Model of Coal Gangue Mixture as Road Base

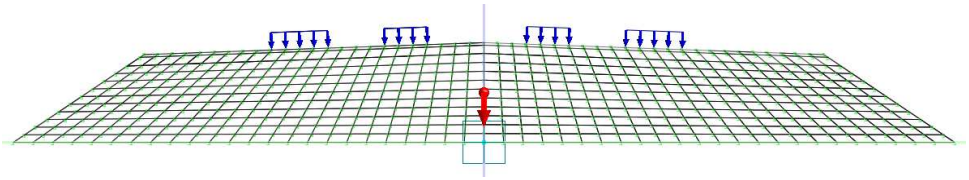
Each layer was represented as a homogeneous, isotropic continuum governed by the Mohr–Coulomb constitutive model. The layer-specific mechanical parameters and their assigned ranges are listed in Table 4.

Table 4 Materials-related parameters used in the model

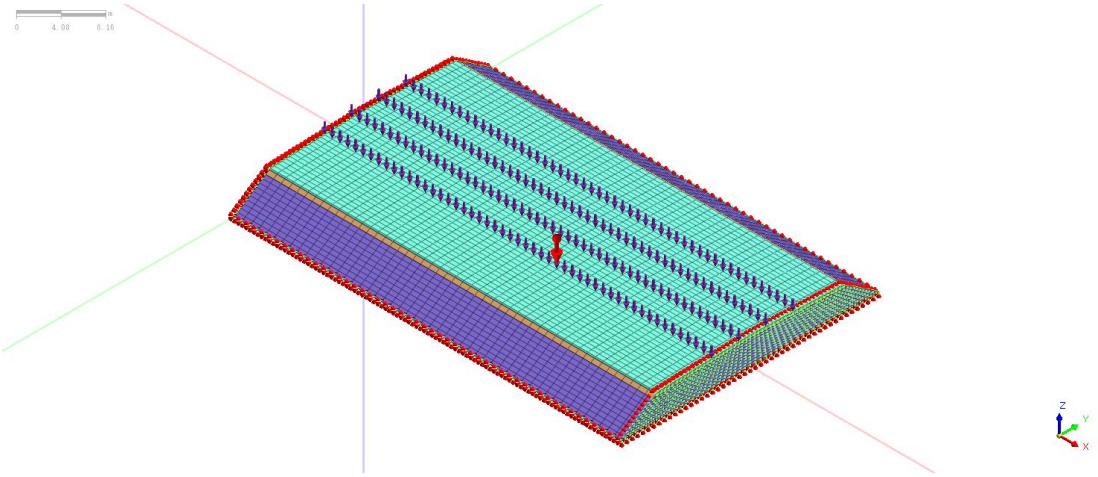
serial number	level	elastic modulus kN/m^2	poisson ratio	volumetric weight kN/m^3	cohesion kN/m^2	internal friction of angle /°
1	surface	1200000	0.35	24.5	500	21.5
2	GFCF mixture	2240000~1490000	0.31~0.26	17.3~16.9	380~640	34~37

3	earth base	80000	0.45	16	65	36

The model comprised 43,600 elements and 60,701 nodes. To limit computational cost, the longitudinal model length in the x direction was set to 50 m. Elastic, viscous, and static boundary treatments were assigned in the numerical implementation, and the moving-load arrangement is shown in Figure 7.



(a) Coal gangue mixture as pavement base road model profile (only show the grid)



(b) Moving-load arrangement for the GFCF pavement-base model

Figure 7 Geometry and moving-load arrangement of the GFCF pavement-base model

The analysis focused on the two-way, four-lane carriageway. Continuous cyclic moving loads were applied along the four traffic lanes in both directions. To isolate the principal traffic-loading effects, temporary and static loads on the shoulder areas were not included.

3.2 Numerical calculation schemes

The measured mechanical properties were used to define fiber-dependent GFCF material parameter sets for comparative simulation. Three groups of calculations were conducted to examine the effects of fiber-dependent material parameters, vehicle speed, and traffic-load magnitude on settlement and vertical stress. These simulations provide relative sensitivity comparisons within the adopted model and do not constitute field validation or code-compliance verification.

Scheme 1—Fiber-dependent material parameters: the GFCF base layer was assigned the parameter sets corresponding to fiber contents of 0.2%, 0.4%, 0.6%, and 0.8%, while aggregate gradation and the coal gangue: fly ash: cement mass ratio were kept constant.

Scheme 2—Vehicle speed: the 0.6% fiber mixture was simulated at 50, 80, and 100 km h^{-1} under the same heavy-traffic load to compare the effect of load residence time and moving speed.

Scheme 3—Traffic-load magnitude: moderate, heavy, and severe traffic-load cases were defined using the vehicle parameters listed in Table 5. With the heavy-load case as the reference, the total vehicle weight for the moderate case was set to 0.6 times the heavy-load value, whereas the severe case was set to 1.4 times the heavy-load value, in accordance with the adopted

interpretation of JTG D40.

Table 5 Model Road Vehicle Design Parameters

Vehicle no.	Total weight (kN)	Applied load (kN)	Front-axle load (kN)	Rear-axle load (kN)	Axle spacing (m)
1	12.50	5.00	3.40	9.10	1.3
2	15.00	4.500	4.60	10.40	1.5
3	15.00	5.00	4.20	10.80	1.6
4	22.00	11.00	5.90	16.10	1.7
5	25.00	15.50	7.50	17.50	1.8
6	80.25	35.00	19.20	61.05	2.0
7	150.60	62.60	35.50	115.10	2.5
8	187.00	100.00	74.80	112.2	--
9	225.40	120.00	89.50	135.90	--
10	146.00	70.00	45.50	100.50	--
11	25.00	15.50	7.50	17.50	1.8
12	18.50	8.90	5.20	13.30	1.8
			cycle		

The same monitoring point was used in all simulations and was located near the centre of an inner traffic lane, as shown in Figure 8. Vertical settlement and vertical stress histories were extracted at this point for each calculation step. The complete simulation matrix is summarized in Table 6.

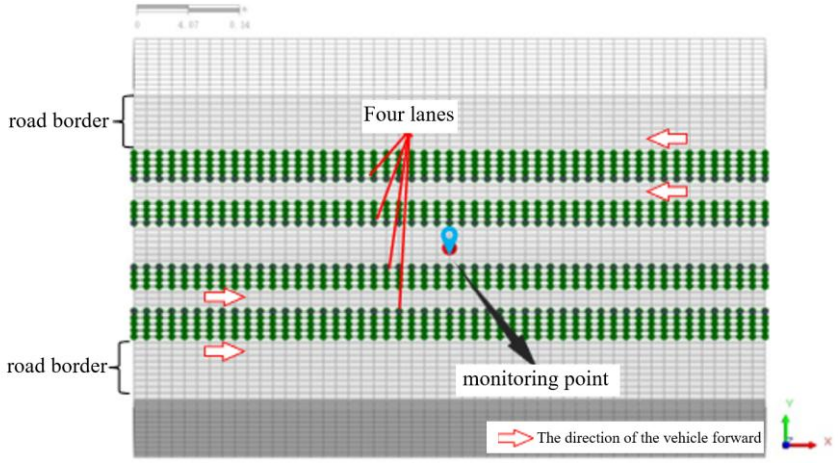


Figure 8 Detection point position layout diagram

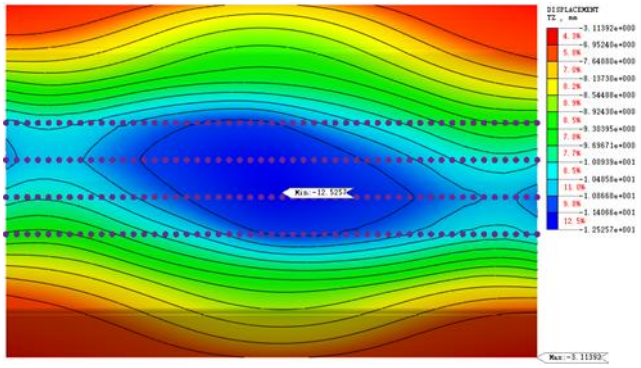
Table 6 Numerical simulation scheme of road settlement law using coal gangue mixture as road base filler

scheme	bed layer filling	Mixture and fiber parameters	Vehicle speed/km/h	Traffic load
1-1	GFCF mixture	n = 0.4, fiber content 0.2 % Coal gangue : fly ash : cement = 82 : 12 : 6	80	Heavy traffic loads
1-2		n = 0.4, fiber content 0.4 % Coal gangue : fly ash : cement = 82 :	80	

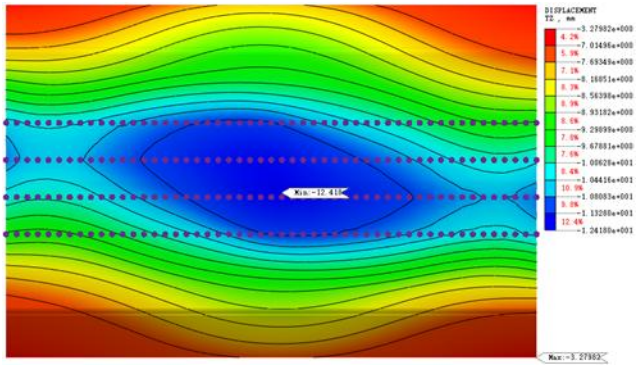
		12 : 6		
1-3	GFCF mixture	n = 0.4, fiber content 0.6 % Coal gangue : fly ash : cement = 82 : 12 : 6	80	Heavy traffic loads
1-4		n = 0.4, fiber content 0.8 % Coal gangue : fly ash : cement = 82 : 12 : 6	80	
2-1	GFCF mixture	n = 0.4, fiber content 0.6 % Coal gangue : fly ash : cement = 82 : 12 : 6	50	Heavy traffic loads
2-2			80	
2-3			100	
3-1	GFCF mixture	n = 0.4, fiber content 0.6 % Coal gangue : fly ash : cement = 82 : 12 : 6	80	Moderate traffic load
3-2			80	Heavy traffic loads
3-3			80	Severe traffic loads

3.3 Numerical simulation of GFCF mixture pavement base material

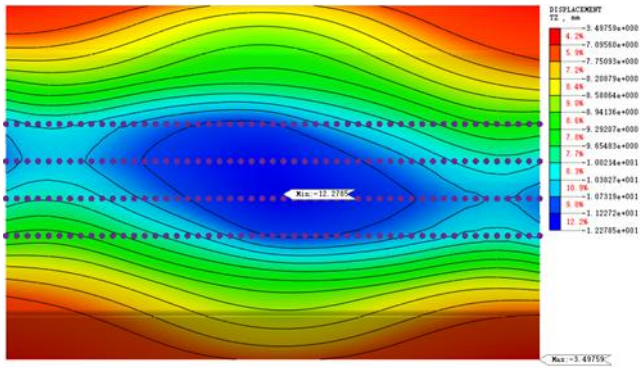
Simulations were conducted for GFCF mixtures containing 0.2%, 0.4%, 0.6%, and 0.8% fiber (Schemes 1-1 to 1-4). The numerical model did not represent individual fibers explicitly; instead, fiber dosage was reflected through the assigned continuum parameters in Tables 4 and 6, while the Talbot index and coal gangue: fly ash: cement ratio were held constant. The resulting settlement contours are shown in Figure 9.



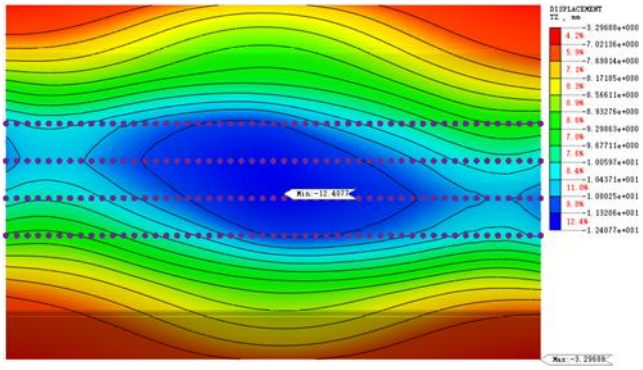
(a) Scheme 1-1 road settlement cloud map



(b) Scheme 1-2 road settlement cloud map



(c) Scheme 1-3 road subsidence cloud map

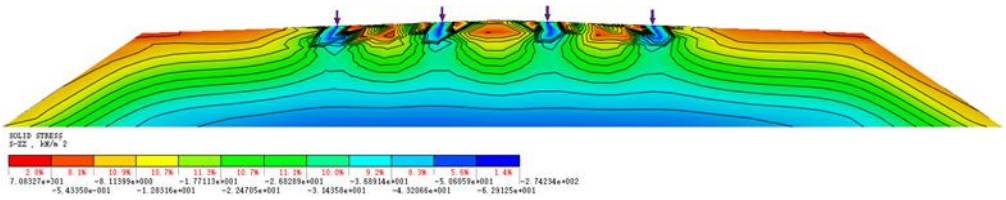


(d) Scheme 1-4 road settlement cloud map

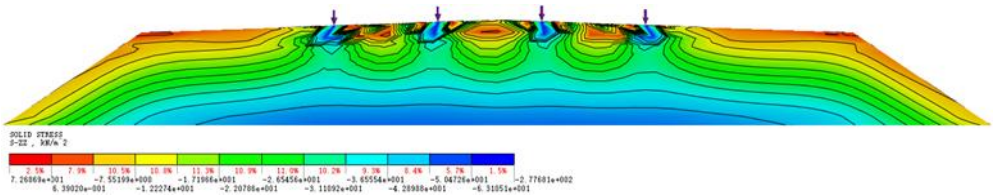
Figure 9 Cloud map of settlement of GFCF mixture base road in Scheme 1

As presented in Figure 9, the maximum settlement of GFCF mixture pavement base material road is 12.53 mm, 12.42 mm, 12.28 mm, and 12.41 mm when the fiber content is 0.2%, 0.4%, 0.6%, and 0.8%, respectively. When the fiber content is 0.6 %, the maximum settlement is smaller than that of other fiber parameters, indicating that the mechanical properties of the material are optimal when the fiber content is 0.6 %. From the settlement value, the fiber content in the test and simulation range will have a certain influence on the road settlement, but the influence is relatively small.

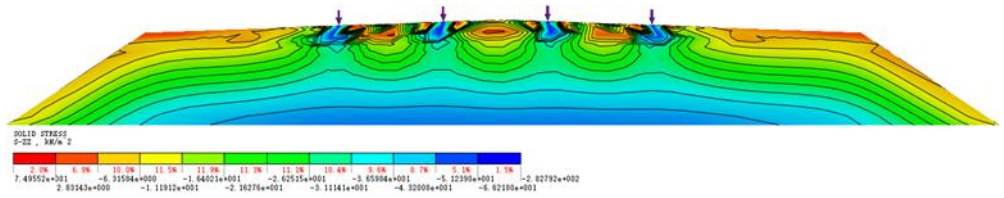
The edge position of the road model is sliced to obtain the vertical stress of the left-view section when driving, as shown in Figure 10.



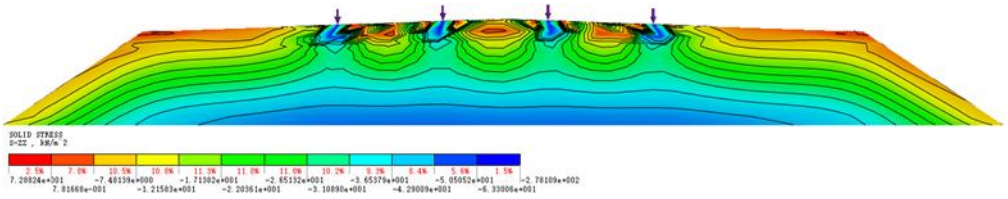
(a) Scheme 1-1 The vertical stress at the left section of the road



(b) Scheme 1-2 The vertical stress of the left section of the road



(c) Scheme 1-3 The vertical stress of the left section of the road

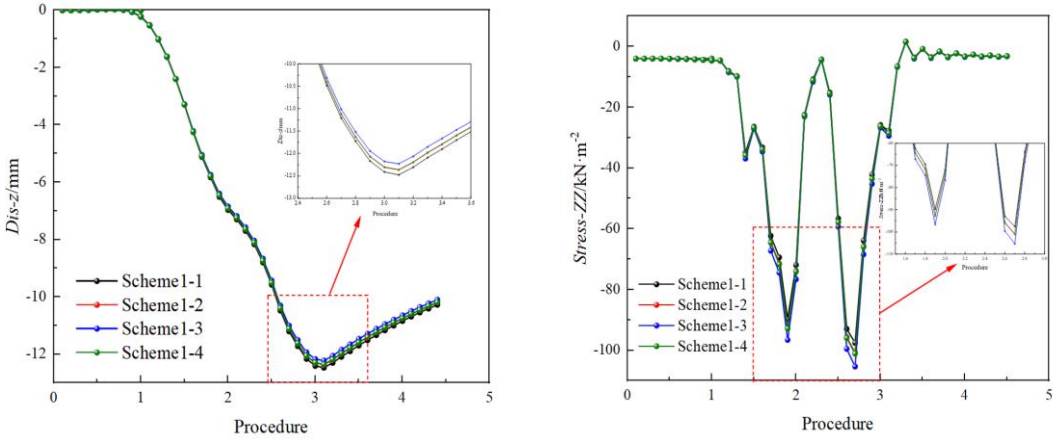


(d) Scheme 1-4 The vertical stress of the left section of the road

Figure 10 Vertical stress at the left section position of the GFCF mixture base road in Scheme 1

As presented in Figure 10, the analysis shows that when the fiber content is 0.2%, 0.4%, 0.6%, and 0.8%, the maximum vertical stress of the GFCF mixture pavement base material road is 274.2kN/m^2,277.6kN/m^2,282.7kN/m^2,278.1kN/m^2, respectively. When the fiber content is 0.6, the vertical stress is the largest. The results obtained by the numerical calculation model confirm that the fiber content of 0.6% in the fiber mixture subgrade ratio, which has the best mechanical properties.

According to the layout of the monitoring point scheme, the vertical settlement value and vertical stress detected under different step values of the above simulation scheme are obtained, and the curve is drawn, as shown in Figure11.



（a）Scheme 1-1 ~ 1-4 measuring point position subsidence law

（b）Scheme 1-1 ~ 1-4 measuring points vertical stress

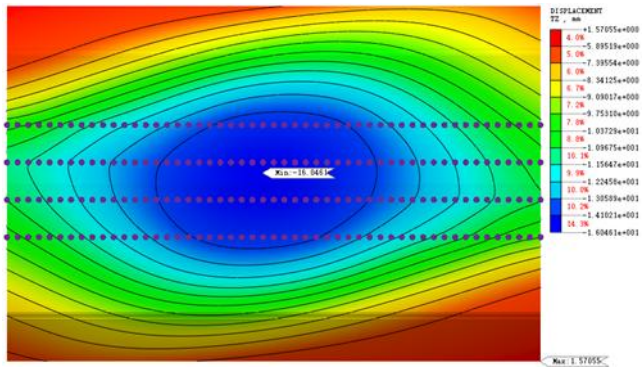
Figure 11 Settlement law and vertical stress of measurement points for GFCF mixture base road in Scheme 1

At the monitoring point (Figure 11), the maximum settlements were 12.47, 12.36, 12.22, and 12.35 mm for fiber contents of 0.2%, 0.4%, 0.6%, and 0.8%, respectively. The 0.6% case again produced the smallest settlement, consistent with the contour-based values in Figure 9. Nevertheless, the differences among the four cases remained small, indicating limited settlement sensitivity to the fiber-dependent parameter sets within the investigated range.

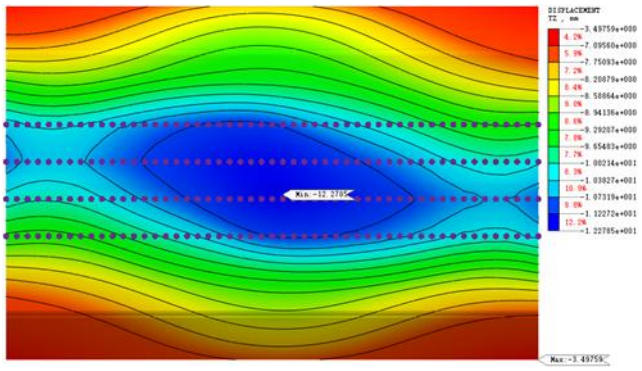
3.4 The influence of vehicle speed on the settlement and stress of GFCF-filled subgrade road

Vehicle speeds of 50, 80, and 100 km/h were simulated in Scheme 2. The GFCF base layer used a Talbot index of 0.4, a fiber content of 0.6%, and a coal gangue: fly ash: cement mass ratio of

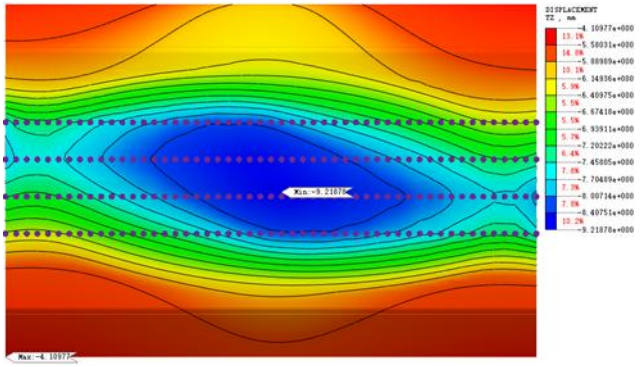
82:12:6. Settlement contours for Schemes 2-1 to 2-3 are shown in Figure 12.



(a) The speed of 50km / h road subsidence cloud



(b) The speed of 80km / h road subsidence cloud

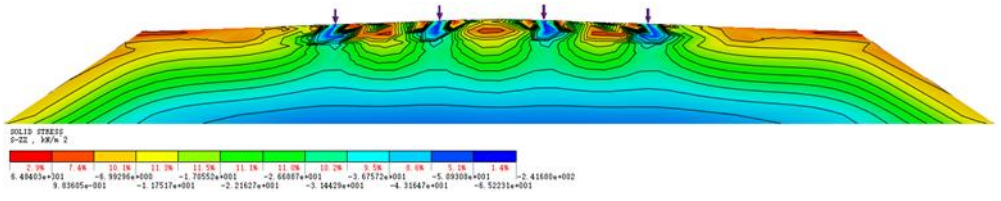


(c) The speed of 100km / h road subsidence cloud

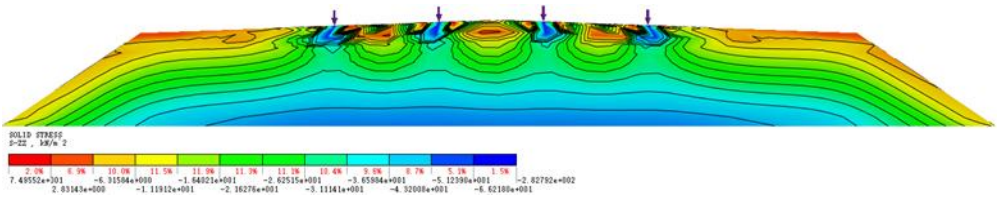
Figure 12 Road settlement of GFCF mixture base under different vehicle speeds

As presented in Figure 12, the maximum road settlement of GFCF mixture pavement base material is 17.15 mm, 12.28 mm, and 9.22 mm, respectively, when the vehicle speed is 50 km/h, 80 km/h, and 100 km / h, respectively. It can be clearly seen that the road settlement of GFCF mixture pavement base material is negatively correlated with the vehicle speed; that is, under the same conditions, the slower the vehicle speed, the greater the road settlement. When the vehicle speed is slow, the vehicle will act on the same position for a long time, so the displacement at this position will be increased.

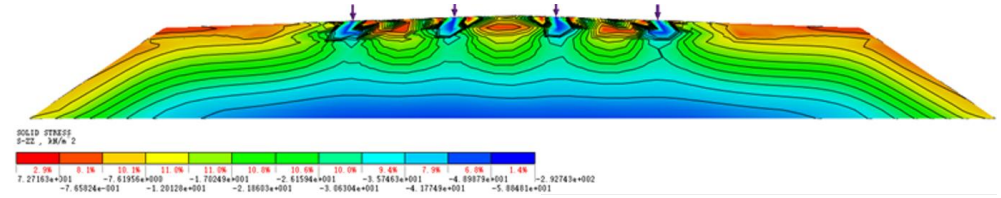
The edge position of the road model is sliced to obtain the vertical stress of the cross-sectional view when driving, as shown in Figure 13.



（a）Speed 50km/h Vertical stress at leftmost section of road



（b）Speed 80km/h Vertical stress at leftmost section of road

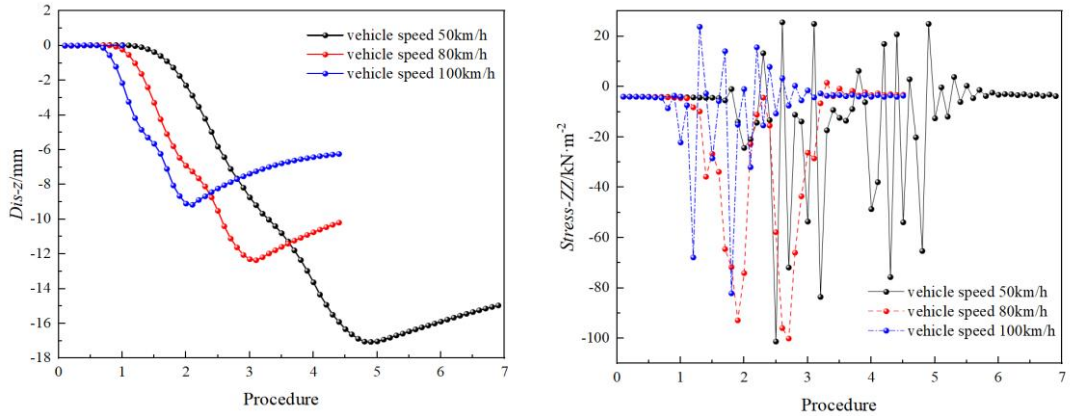


（c）Speed 100km/h Vertical stress at leftmost section of road

Figure 13 Leftmost section position of GFCF mixture base under different vehicle speeds

As presented in Figure 13, when the vehicle speed is 50km/h, 80km/h and 100km/h, the maximum vertical stress on the side of the road of GFCF mixture pavement base material is 241.68kN/ m^2, 282.79kN/m^2 and 292.74kN/m^2respectively. To a certain extent, the greater the vehicle speed, the greater the vertical stress on the road. Therefore, speed control is an important means to slow down road damage.

According to the layout of the monitoring point scheme, the vertical settlement value and vertical stress detected under different step values of the above simulation scheme are obtained, and the curve is drawn, as shown in Figure14.



(a) Settlement law of measuring point position at different speeds

(b) The vertical stress of the measuring point at different speeds

Figure 14 Settlement Law and Vertical Stress of Measurement Points at Different Vehicle Speeds

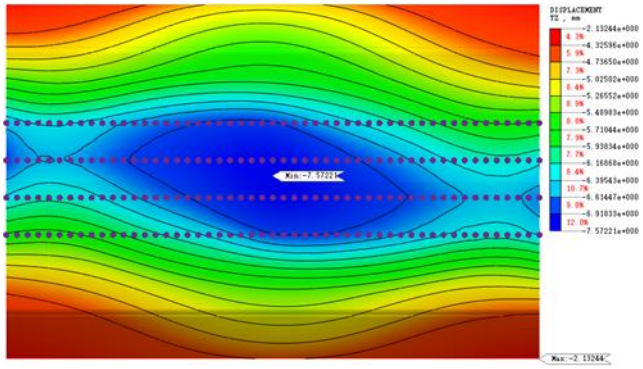
At the monitoring point, the maximum settlements were 17.06, 12.22, and 9.16 mm at 50, 80, and 100 km/h, respectively (Figure 14a), confirming the same speed-dependent settlement ranking as Figure 12. The monitoring-point stress histories in Figure 14b show lower local peak stress at

higher speed, whereas Figure 13 reports the maximum stress over the extracted section. These metrics need not vary identically because they refer to different spatial locations and extraction definitions. Overall, the speed-induced settlement range was substantially larger than the settlement differences among the four fiber-dependent parameter sets.

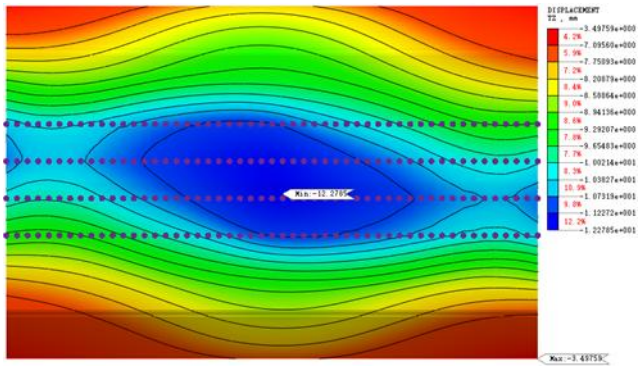
3.5 The influence of traffic load on the settlement and stress of GFCF-filled subgrade road

Scheme 3 considered moderate, heavy, and severe traffic-load cases. The GFCF base layer retained a Talbot index of 0.4, a fiber content of 0.6%, and a coal gangue: fly ash: cement mass ratio of 82:12:6.

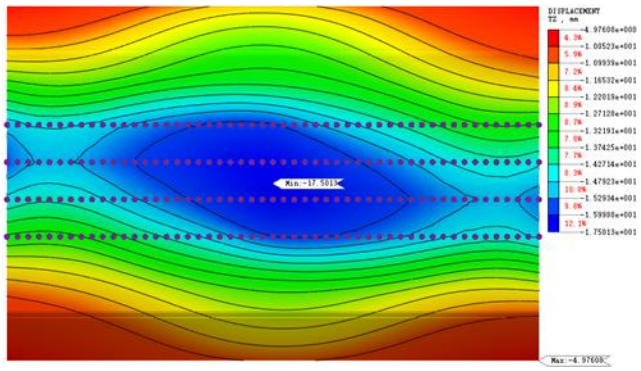
Settlement contours for the moderate, heavy, and severe load cases (Schemes 3-1 to 3-3) are shown in Figure 15.



(a) Road settlement cloud map of moderate traffic load



(b) Road settlement cloud map under heavy traffic load



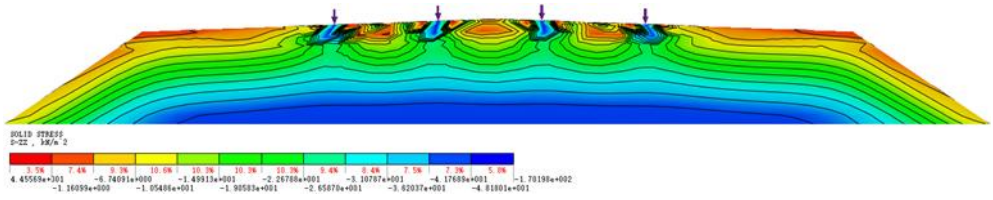
(c) Road settlement cloud map under severe traffic load

Figure 15 Road settlement of GFCF mixture base under different traffic loads

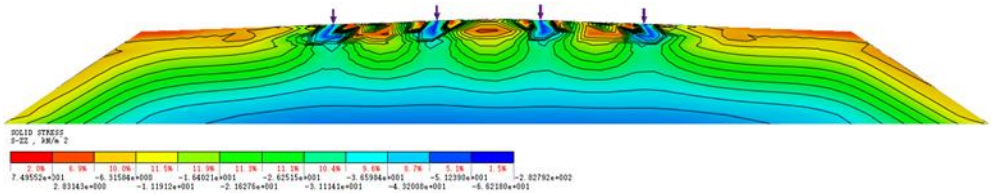
As presented in Figure 15, the maximum settlement of GFCF mixture pavement base material road under moderate traffic load, heavy traffic load, and severe traffic load is 7.57 mm, 12.28 mm, and 17.50 mm, respectively. With the increase in traffic load conditions, the maximum settlement

of the GFCF mixture pavement base material road is positively correlated. The more serious the traffic load, the greater the road settlement, and the impact of traffic load is extremely serious.

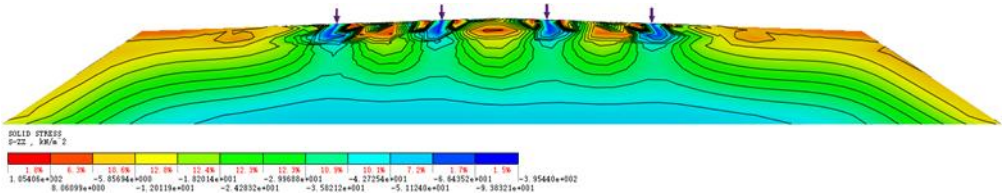
The edge position of the road model is sliced to obtain the vertical stress of the left-view section when driving, as shown in Figure 16.



(a) The vertical stress of the leftmost section of the road under moderate traffic load



(b) Vertical stress on the leftmost section of heavy traffic load road.

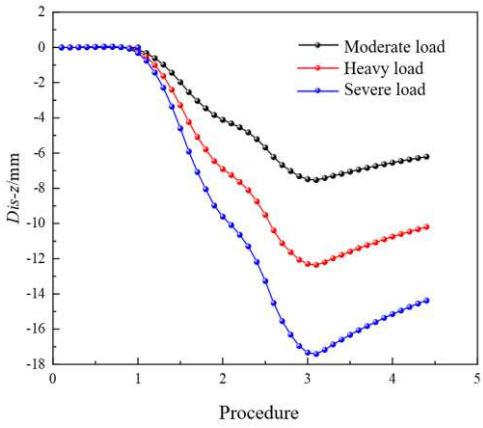


(c) The vertical stress of the leftmost section of the road under severe traffic load

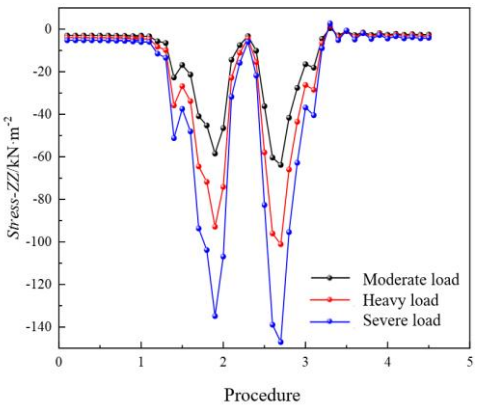
Figure 16 Leftmost section position of GFCF mixture base under different traffic loads

As presented in Figure 16, under the conditions of moderate traffic load, heavy traffic load and severe traffic load, the maximum stress in the vertical direction of the road side of the GFCF mixture pavement base material is 170.20kN/m^2,282.7kN/m^2 and 395.44kN m^2 respectively. The vertical stress of the road is also positively correlated with the traffic load, so the load control is also an important factor affecting the road damage.

Settlement and vertical stress at the monitoring point were obtained for various loading steps, and the corresponding relationship is presented in Figure 17.



（a）Settlement law of measuring point position under different traffic loads



（b）The vertical stress of the measuring point under different traffic loads

Figure17 Settlement law and vertical stress of measurement points under different traffic loads

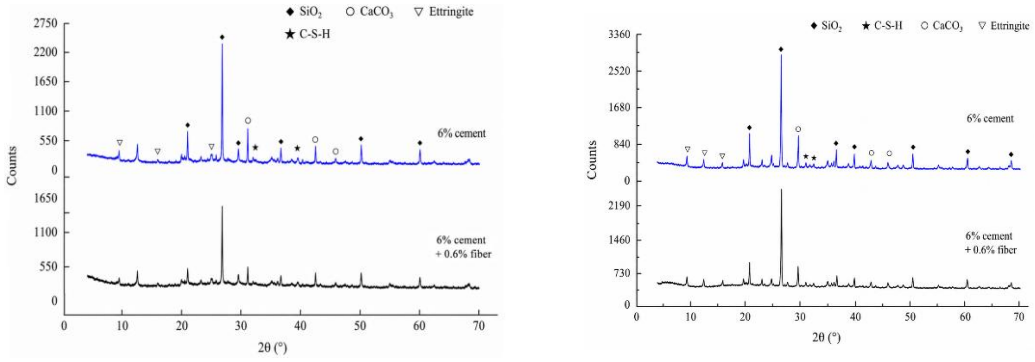
At the monitoring point, the maximum settlements were 7.57, 12.22, and 17.50 mm under moderate, heavy, and severe traffic loads, respectively (Figure 17a). The corresponding monitoring-point peak stresses were 63.82 kN/m^2, 101.44 kN/m^2, and 147.06 kN/m^2 (Figure 17b). These values are lower than the section-level maxima in Figure 16 because they refer to a single monitoring location. Both settlement and local peak stress increased with traffic-load magnitude.

The numerical results demonstrate that the adopted GFCF parameter sets can be examined within a pavement-scale moving-load model and that settlement is more sensitive to vehicle speed and traffic-load magnitude than to the comparatively small differences among the fiber-dependent material sets.

4 Discussion

4.1 Phase Evolution Revealed by XRD

XRD patterns were obtained for the 6% cement GFC mixture and the corresponding GFCF mixture containing 0.6% basalt fiber after 7 and 28 d of curing. The results are presented in Figure 18.



(a) 7 d (b) 28 d

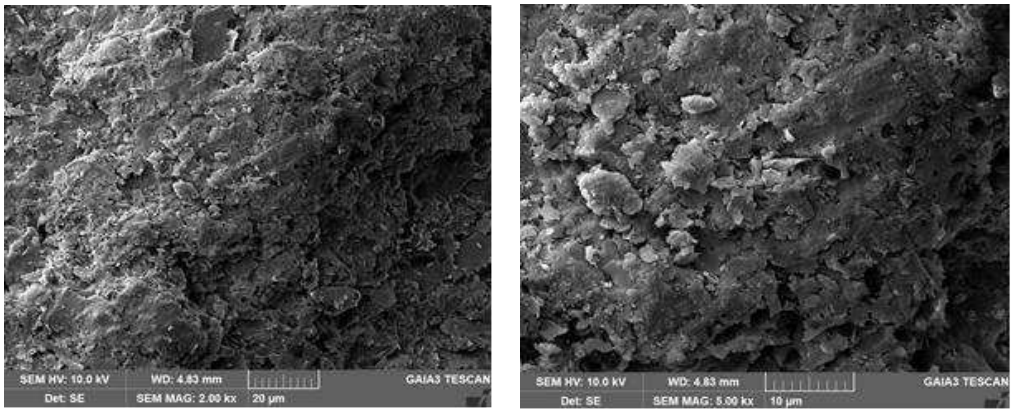
Figure 18. XRD patterns of the 6% cement GFC and 6% cement GFCF mixture containing 0.6% basalt fiber after (a) 7 d and (b) 28 d of curing

The patterns are dominated by SiO2 reflections, with weaker peaks tentatively associated with CaCO3 and ettringite-related phases. A distinct C-S-H peak is not expected because C-S-H is poorly crystalline or largely amorphous. Because the patterns use separate local intensity scales and no internal standard, Rietveld refinement, or other quantitative phase analysis, differences in peak height are interpreted qualitatively; the results are consistent with continued reaction-product development.

4.2 SEM Evidence of Matrix Densification and Fiber–Matrix Interaction

4.2.1 Raw Gangue Morphology and Fiber Contact

For SEM preparation, blocks smaller than 10 mm were collected from the interiors of cured specimens. One surface was flattened when necessary, while the observation surface was retained as a natural fracture surface. Each specimen was mounted on conductive adhesive and gold-coated before imaging. SEM was used to examine pore filling, particle bonding, and fiber–matrix interaction. The raw coal gangue was first characterized to identify surface features that could influence subsequent bonding with the cementitious matrix, as shown in Figure 19.



（a）2000X　　（b）5000X

Figure 19 Microscopic morphology of coal gangue

Figure 19 shows that the raw coal gangue consists of irregular, angular, and locally lamellar particles with rough surfaces, stepped edges, pores, and micro-scale discontinuities. These surface irregularities increase the available contact area and provide potential nucleation and mechanical-interlocking sites for hydration products. However, unfilled pores, microcracks, and cleavage planes may concentrate stress and promote crack initiation along weak particle boundaries. Continued hydration can progressively fill these defects and improve the continuity of the gangue–matrix interface.

The fiber–matrix interface was subsequently examined to determine whether the basalt fibers were embedded in and connected to the surrounding cementitious phase. Representative morphologies are shown in Figure 20.

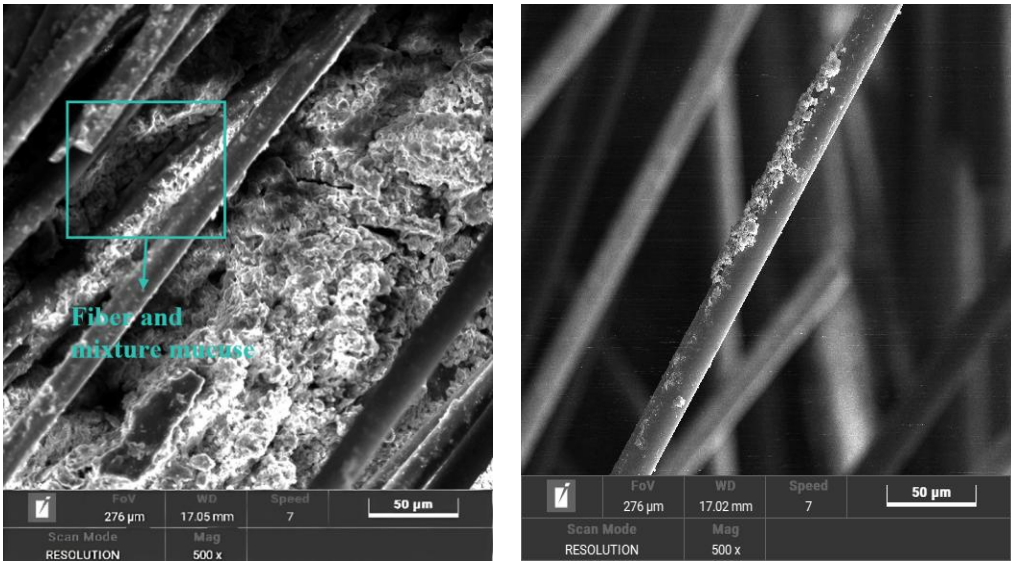
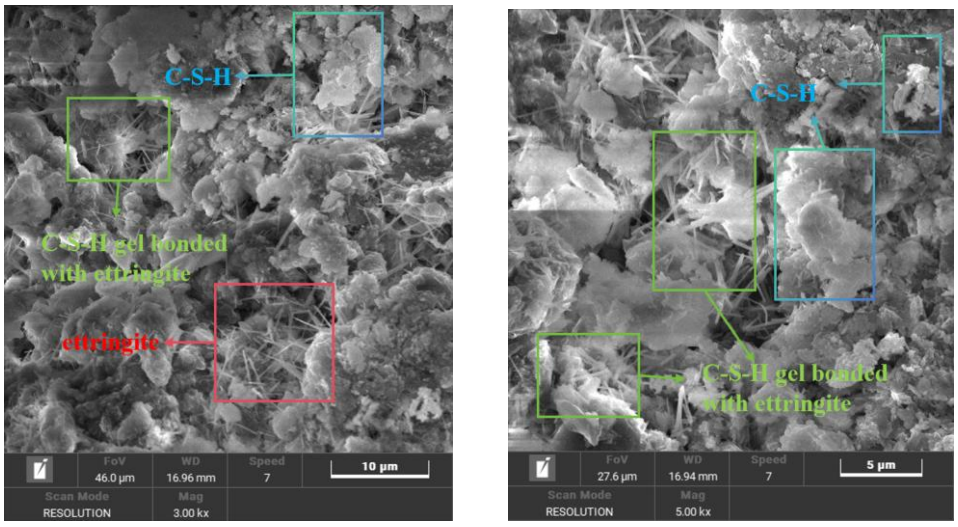


Figure 20 Fibers in the GFCF mixture(500x)

Figure 20 shows basalt fibers in contact with the surrounding matrix and with adhered fine particles. These features are consistent with possible mechanical anchorage, stress transfer, and crack bridging. However, SEM morphology alone does not quantify interfacial bond strength or establish the magnitude of the fiber-induced mechanical improvement.

4.2.2 Curing-Age-Dependent Matrix Densification

To examine the development of the cementitious skeleton, the GFCF mixture containing 0.6% basalt fiber was observed after 7 and 28 d. The 7 d morphology is presented in Figure 21.

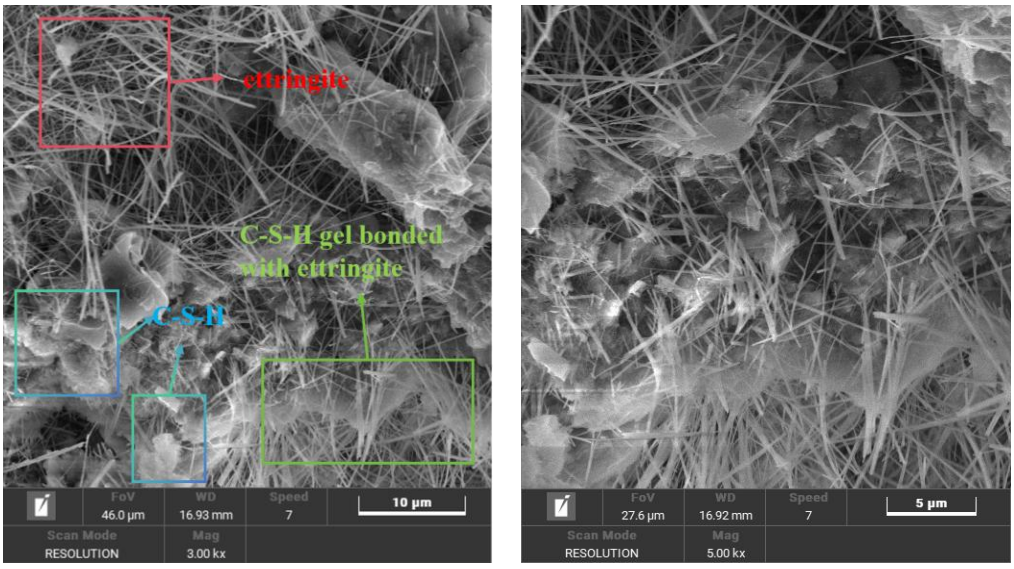


（a）3000x　　（b）5000x

Figure 21 Fiber addition of 0.6%, microstructure of 7d GFCF mixture

At 7 d, partially exposed gangue particles, visible open spaces, dispersed needle-like products, and discontinuous gel-like regions are observed. These features indicate that an early cementitious skeleton had formed but remained incompletely connected. The needle-like and gel-like morphologies are consistent with ettringite-related and C–S–H-rich products, respectively.

The corresponding 28 d morphology was examined to determine whether the discontinuous early-age products developed into a denser and more continuous matrix in Figure 22.



（a）3000x　　（b）5000x

Figure 22 Fiber addition of 0.6%, microstructure of 28d GFCF mixture

Compared with the 7d specimens, the 28d matrix contains more extensively intergrown needle-like and gel-like products, while the number and size of visible open voids are reduced. The denser morphology is consistent with continued cement hydration, later-age fly-ash reaction, and improved contact among reaction products, gangue particles, and basalt fibers. Nevertheless, morphology

alone does not provide quantitative porosity or phase-content information. The combined mechanical and microstructural observations suggest a coupled mechanism in which reaction products improve particle bonding and dispersed basalt fibers may redistribute tensile stress and bridge developing cracks.

5 Conclusions

Based on laboratory testing, microstructural characterization, and numerical simulation, the mechanical response, deformation behavior, and possible reinforcement mechanism of gangue–fly ash–cement–fiber pavement-base materials were evaluated. The principal conclusions are as follows:

(1) Unconfined compressive strength and splitting tensile strength showed the same nonlinear response to fiber content, increasing from 0.2% to 0.6% and then decreasing at 0.8%. The 0.6% mixture achieved the highest unconfined compressive strengths of 10.27 MPa at 7 d and 14.47 MPa at 28 d, together with the highest splitting tensile strengths of 0.91 and 1.51 MPa, respectively. Thus, 0.6% was the best-performing strength dosage within the investigated range.

(2) Compressive resilient modulus decreased monotonically as fiber content increased. The modulus fell from 882 MPa to 794 MPa at 7 d and from 1497 MPa to 1287 MPa at 28 d as fiber content increased from 0.2% to 0.8%. Basalt fiber therefore produced a strength–stiffness trade-off rather than a uniform improvement in all mechanical properties.

(3) The modeled maximum settlements for the 0.2%, 0.4%, 0.6%, and 0.8% fiber-dependent parameter sets were 12.53 mm, 12.42 mm, 12.28 mm, and 12.41mm, respectively, showing only limited sensitivity to fiber content. In comparison, increasing vehicle speed from 50 km/h to 100 km/h reduced settlement from 17.15 mm to 9.22 mm, whereas increasing traffic load from moderate to severe raised settlement from 7.57 mm to 17.50 mm. Vehicle speed and traffic-load magnitude therefore had greater modeled effects than the differences among the fiber-dependent material sets.

(4) XRD and SEM observations were consistent with continued reaction-product development and a denser matrix at 28 d than at 7 d. The observed fiber–matrix contact and adhered particles also suggest possible mechanical anchorage and crack bridging, although these mechanisms were not quantified directly.

Author Contributions: Peng Huang: Conceptualization, Methodology, Software, Validation, Formal analysis, Resources, Data curation, Writing - original draft, Writing - review & editing, Supervision, Project administration, Funding acquisition. Qihe Lan: Validation, Formal analysis, Investigation, Data curation, Writing - original draft, Writing - review & editing, Visualization. Erkan Topal: Investigation, Writing - review & editing. Hu Shao: Conceptualization, Methodology, Validation, Investigation, Writing - review & editing. Zhenjiang You: Writing - review & editing. Chengyi Zhao: Formal analysis, Writing - review & editing. Shuxuan Ma: Writing - review & editing.

Funding: This work was supported by the National Natural Science Foundation of China (Project No. 52474111)

Institutional Review Board Statement: Not applicable

Informed Consent Statement: Not applicable

Data Availability Statement: The data presented in this study are available on request from the corresponding author.

Conflicts of Interest: The authors declare no conflicts of interest.

References:

[1] Bian, Z.; Dong, J.; Lei, S.; Leng, H.; Mu, S.; Wang, H. The Impact of Disposal and Treatment of Coal Mining Wastes on Environment and Farmland. *ENVIRONMENTAL GEOLOGY* **2009**, *58*, 625–634, doi:10.1007/s00254-008-1537-0.

[2] Duan, X.; Xia, J.; Yang, J. Influence of Coal Gangue Fine Aggregate on the Microstructure of Cement Mortar and Its Action Mechanism. *Journal of Building Materials* 2014, 17, 700–705.

[3] Ma, J.; Yu, Z.M.; Shu, S.H.; Zeng, Z.H. Environmental Hazards of Coal Gangue and Control Measures. *Coal Engineering* 2015, 47, 70–73.

[4] Gong C.; Yan J.; Liu J.; Yu H. Biology Migration and Distribution Characteristics of Trace Elements in Reconstructed Soil with Coal Gangue Filling *Agricultural Science & Technology* **2016**, *17*, doi:10.16175/j.cnki.1009-4229.2016.09.043.

[5] Wang, S.; Luo, K.; Wang, X.; Sun, Y. Estimate of Sulfur, Arsenic, Mercury, Fluorine Emissions Due to Spontaneous Combustion of Coal Gangue: An Important Part of Chinese Emission Inventories. *ENVIRONMENTAL POLLUTION* **2016**, *209*, 107–113, doi:10.1016/j.envpol.2015.11.026.

[6] Qin, J.; Zhao, R.; Chen, T.; Zi, Z.; Wu, J. Overview on Co**-**Combustion of Coal and Municipal Solid Waste in a Circulating Fluidized Bed. *SHANDONG ELECTRIC POWER* **2021**, *48*, 64–67.

[7] Moghadam, M.; Ajalloeian, R.; Hajiannia, A. Preparation and Application of Alkali-Activated Materials Based on Waste Glass and Coal Gangue: A Review. *CONSTRUCTION AND BUILDING MATERIALS* **2019**, *221*, 84–98, doi:10.1016/j.conbuildmat.2019.06.071.

[8] Jia, J.; Ma, N ; Dong, Y; Li, Q ; Zhang, D. Review on The Comprehensive Utilization of Coal Gangue. *Clean Coal Technology* **2024**, *30*, 36–45, doi:10.13226/j.issn.1006-6772.23112701.

[9] Yellishetty, M.; Karpe, V.; Reddy, E.; Subhash, K.; Ranjith, P. Reuse of Iron Ore Mineral Wastes in Civil Engineering Constructions: A Case Study. *RESOURCES CONSERVATION AND RECYCLING* **2008**, *52*, 1283–1289, doi:10.1016/j.resconrec.2008.07.007.

[10] Marland, S.; Han, B.; Merchant, A.; Rowson, N. The Effect of Microwave Radiation on Coal Grindability. *FUEL* **2000**, *79*, 1283–1288, doi:10.1016/S0016-2361(99)00285-9.

[11] Li, W.; Wang, D.; Niu, J.; Ma, X. Preparation of Coal Gangue Cement Mortar.; Gan, B., Gan, Y., Yu, Y., Eds.; 2013; Vol. 684, pp. 159-+.

[12] Dong, Z.; Xia, J.; Fan, C.; Cao, J. Activity of Calcined Coal Gangue Fine Aggregate and Its Effect on the Mechanical Behavior of Cement Mortar. *CONSTRUCTION AND BUILDING MATERIALS* **2015**, *100*, 63–69, doi:10.1016/j.conbuildmat.2015.09.050.

[13] Qiu, Y.; Zhang, X.; Liu, K.; Hu, X.; Guan, B. Research on Mechanical Behaviour of Cement Mortar with High-Volume Coal Gangue.; Zhao, J., Ed.; 2011; Vol. 261–263, pp. 685-+.

[14] Wang, D.; Zuo, Y.; li, Q ; fan, D.; Cui, Y. ; wang, Wen. Mineralogical Characteristics of Coal Gangue and Resource Utilization of Building Materials. *BRICK-TILE* **2006**, 17–23.

[15] Wu, J ; Gao, W.; Zhang, Z.; Tang, X.; Yi, M. Study on Strength and Deformation Characteristics of Coal Gangue Subgrade Filling. *Journal of Railway Science and Engineering* **2021**, *18*, 885–891, doi:10.19713/j.cnki.43-1423/u.T20200536.

[16] Wen, P.; Wang, C.; Song, L.; Chen, H.; Chen, M. A Comprehensive Evaluation on Particles Breakage Characteristics of Waste Argillaceous Gangue as Subgrade Filler. ROAD MATERIALS AND PAVEMENT DESIGN 2025, 26, 477–496, doi:10.1080/14680629.2024.2356798.

[17]Hui, B.; Hui, Y.; Zhang, X.; Zhang, W.; Yan, S.; Men, G. STUDY ON STRESS CHARACTERISTICS OF HIGH-POROSITY COAL GANGUE SUBGRADE DURING FILLING PROCESS. JOURNAL OF THEORETICAL AND APPLIED MECHANICS 2023, 61, 625–641, doi:10.15632/jtam-pl/168989.
[18] Zhang, H.; Lei, J.; Wu, Q.; Tian, X. Study on the Permanent Deformation and Dynamic Stress-Strain of Coarse-Grained Subgrade Filler under Cyclic Loading. BUILDINGS 2024, 14, doi:10.3390/buildings14072092.
[19] Li, J.; Wang, J. Comprehensive Utilization and Environmental Risks of Coal Gangue: A Review. JOURNAL OF CLEANER PRODUCTION 2019, 239, doi:10.1016/j.jclepro.2019.117946.
[20]Zheng, Q.; Zhou, Y.; Liu, X.; Liu, M.; Liao, L.; Lv, G. Environmental Hazards and Comprehensive Utilization of Solid Waste Coal Gangue. PROGRESS IN NATURAL SCIENCE-MATERIALS INTERNATIONAL 2024, 34, 223–239, doi:10.1016/j.pnsc.2024.02.012.
[21]Gao, L.; Liu, Y.; Xu, K.; Bai, L.; Guo, N.; Li, S. A Short Review of the Sustainable Utilization of Coal Gangue in Environmental Applications. RSC ADVANCES 2024, 14, 39285–39296, doi:10.1039/d4ra06071g.
[22] Cheng, Y.; Wang, H.; Wang, Y. Preliminary Research on Carbonation Resistance of Fiber Reinforced Concrete. *JOURNAL OF BUILDING MATERIALS* **2010**, *13*, 792–795.
[23] Tan, L; Zeng, D.; Zhao, P;, Yu, S; Zhang Z.; Lin X; Wang X. Modification test of basalt fiber reinforced concrete and its application in subsidence area. *Water Resources and Hydropower Engineering* **2024**, *55*, 746–752, doi:10.13928/j.cnki.wrahe.2024.S2.112.
[24] Lang, L. Study on Crack Arrest and Fracture Parameters of Fine Aggregate Concrete Under Impact Loads. *Doctoral Dissertation of Sichuan University*, 2024.
[25]Wang, J; Zhu,Y.; Yan, C.; Zhang, H. Experimental Study on Road Performance of Soil-rock Mixture of Collapsible Loess Mixed with Coal Gangue Roadbed. *Subgrade Engineering* **2021**, 65–68, doi:10.13379/j.issn.1003-8825.202008028.
[26] Guo, Y.; Gao, D.; Ding, C.; Pi, H. Effect of High Steel Fiber Volume Fraction on the Mechanical Properties of Ultrahigh-Performance Concrete Incorporating Entirely Recycled Fine Aggregates. *J. Mater. Civ. Eng.* **2025**, *37*, 04025255, doi:10.1061/JMCEE7.MTENG-20250.
[27] Chen, S. Study on Application of Composite Activated Coal Gangue in Pavement Engineering *Master 's thesis, Southeast University*, 2022.
[28] Yan, G.; Zhou, M.; Chen, X; Yu, G ; Liu, B.; Kang, Z. Study on Application of Coal Gangue Aggregate Pavement Base Material. *Journal of Wuhan University of Technology (Transportation Science & Engineering)* **2021**, *45*, 568–573.
[29] Zhang, W.; Yan, S. Experimental Study on Permeability Modification of Sand-gravel Cladding Soil for Coal Gangue Roadbed. *CONSTRUCTION QUALITY* **2023**, *41*, 84–87.
[30] Zheng, Y.; Zhang, P.; Cai, Y.; Jin, Z.; Moshtagh, E. Cracking Resistance and Mechanical Properties of Basalt Fibers Reinforced Cement-Stabilized Macadam. *Composites Part B: Engineering* 2019, 165, 312–334. doi:10.1016/j.compositesb.2018.11.115.
[31] Wang, X.; He, J.; Mosallam, A.S.; Li, C.; Xin, H. The Effects of Fiber Length and Volume on Material Properties and Crack Resistance of Basalt Fiber Reinforced Concrete (BFRC). *Advances in Materials Science and Engineering* 2019, 2019, 7520549. doi:10.1155/2019/7520549.
[32] Al-Rousan, E.T.; Khalid, H.R.; Rahman, M.K. Fresh, Mechanical, and Durability Properties of

Basalt Fiber-Reinforced Concrete (BFRC): A Review. *Developments in the Built Environment* 2023, 14, 100155. doi:10.1016/j.dibe.2023.100155.

[33] Zhao, Y.; Yang, X.; Zhang, Q.; Liang, N.; Xiang, Y.; Qin, M. Crack Resistance and Mechanical Properties of Polyvinyl Alcohol Fiber-Reinforced Cement-Stabilized Macadam Base. *Advances in Civil Engineering* 2020, 2020, 6564076. doi:10.1155/2020/6564076.

[34] Wiranata, D.Y.; Yang, S.H.; Akgul, C.M.; Hsien, H.Y.; Nugraha, M.Z.P. Use of Coal Ash Cement Stabilized Material as Pavement Base Material: Laboratory Characterization and Field Evaluation. *Construction and Building Materials* 2022, 344, 128055. doi:10.1016/j.conbuildmat.2022.128055.

[35] Yan, P.; Ma, Z.; Li, H.; Gong, P.; Xu, M.; Chen, T. Laboratory Tests, Field Application and Carbon Footprint Assessment of Cement-Stabilized Pure Coal Solid Wastes as Pavement Base Materials. *Construction and Building Materials* 2023, 366, 130265. doi:10.1016/j.conbuildmat.2022.130265.